UDC 621.793:669.295

S. H. Din[1, *], M. A. Shah[2], N. A. Sheikh[1]
[1]Department of Mechanical Engineering,
National Institute of Technology, Srinagar, 190006, India
[2]Department of Physics, National Institute of Technology,
Srinagar, 190006, India
**sajad_08phd12@nitsri.net*

Tribological performance of titanium alloy Ti–6Al–4V via CVD-diamond coatings

In the present study, HFCVD nanocrystalline, microcrystalline and boron-doped nanocrystalline diamond coatings have been deposited on titanium alloy. The effect of boron doping on coefficient of friction and residual stresses of diamond coatings have been studied. The tribological characteristics of the aforementioned three coatings on Ti–6Al–4V substrates were studied using ball on disc micro-tribometer, the thickness of the coatings being 3 μm. The coated Ti–6Al–4V discs were slid against alumina (Al_2O_3) balls with normal load ranging from 1 to 10 N. The boron-doped NCD coated sample disc was found to possess the lowest average coefficient of friction ~ 0.0804 while the undoped NCD and MCD coated sample discs were found to possess the average coefficients of friction of ~ 0.143 and ~ 0.283, respectively. Raman spectroscopy studies revealed that the residual stresses in boron-doped nanocrystalline coatings were tensile in nature, while the residual stresses in undoped NCD and MCD were found to be of compressive nature.

***Keywords**: boron doping, CVD diamond coatings, friction coefficient.*

INTRODUCTION

Titanium and its alloys are widely used in dental and load-bearing bio-implants, owing to their advantageous properties such as low density, low modulus, high strength-to-weight ratio, exceptional fatigue strength, and outstanding formability, as well as superior biocompatibility and corrosion resistance [1–3]. A deposition on a surface is achieved by the chemical vapor deposition method which involves a gas phase. A chemical reaction occurs above the solid surface. For producing diamond films, all chemical vapor deposition techniques require a means of actuating gas-phase carbon comprising precursor molecules [4, 5]. Diamond thin films have been deposited using a variety of chemical vapor deposition techniques, which include hot filament, microwave chemical vapor deposition, RF plasma, and DC jet [6–9]. Substrate conditions, which include the surface preparation procedure, play an important role in the diamond nucleation on a given substrate. In order to enhance the density of diamond nuclei, scratching the substrate with diamond grit is quite effective. The scratching results in diamond residual particles which provide seeds for diamond growth [10]. The hot filament chemical vapor deposition technique possesses many advantages over other methods, being much simpler and easier to adopt for a large-area deposition at a lower cost, which is of special interest for many applications [11].

Due to the high specific strength, biocompatibility, and corrosion resistance, the titanium finds wide application in aerospace, biomedicine and chemical

engineering [12–14]. By the chemical vapor deposition diamond films wear loss can be reduced, since highly adherent diamond coatings can be deposited on titanium [15–16]. The effect of doping on the mechanical properties of diamond films have not been investigated thoroughly [17–20]. Hence in order to broaden the applications of doped diamond films, tribological properties need to be investigated. Boron atoms can be easily incorporated into the diamond lattice, which forms a *p*-type semiconductor with tunable electrical conductivity. Boron-doped diamond has been extensively researched in electrical and semiconductor materials [21–23]. A real application of boron-doped diamond on titanium is its usage as an electrode material. By doping the chemical vapor deposited diamond film with some impurities as boron, nitrogen, or sulphur, the wide gap of diamond (5.5 eV) can be reduced, producing a semiconductor material. Principally, boron-doped diamond has achieved good results for semiconductor sensor applications, both in the solid-state electronics along with electrochemistry. The diameter film properties with high mobility of carriers, higher thermal conductivity, electrical consistency and compatibility with aggressive media, can be widely explored in sensors for toxic gases and also for electrodes for hostile chemical environments [24–29]. It can be found that the tribological properties of boron-doped diamond films on titanium are not clear.

In the present communication, the tribological properties of nanocrystalline diamond films, microcrystalline diamond films and boron-doped diamond films deposited on titanium alloy (Ti–6Al–4V) are investigated. Smooth and adhesive coatings were deposited on titanium alloy substrates, with a thickness of 3 μm. The substrates were chemically etched and deposition was done with hot filament chemical vapor deposition technique. Three types of samples were prepared separately, namely, nanocrystalline diamond coatings, microcrystalline diamond coatings and boron-doped nanocrystalline diamond coatings. Raman spectroscopy technique was used to identify the nature and estimation of residual stresses, and to identify the boron content of a diamond film. The tribological properties are compared. We focus on the tribological behavior of diamond films on titanium alloy in ambient air. Systematic investigation of the relationship between applied normal load and frictional coefficient was carried out to better understand the tribological behavior of the nanocrystalline, microcrystalline, and boron-doped nanocrystalline diamond coatings.

EXPERIMENTAL DETAILS

The nanocrystalline, microcrystalline and boron-doped diamond films are deposited using hot filament chemical vapor deposition apparatus, in separate experiments. The precursor of boron is trimethyl borate ($C_3H_9BO_3$). Titanium alloy samples of diameter 25 and 3 mm thickness in dimensions were slided using silicon carbide (SiC) and cleaned with deionized water. The samples were etched in the solution of HF: H_2SO_4: DI water, rinsed in deionized water three times for 3 min each and blown dry with air gun. The mirror finish was obtained by polishing the samples with diamond paste (2.0, 1.0 and 0.5 μm). An ultrasonicator was used to clean the samples with acetone for 30 min and then dried thoroughly by a hot drier. Dimethyl sulphoxide (DMSO) solution containing diamond seedings of size 4 μm were used. Before deposition of nanodiamond films, the titanium samples were dispersed in it. This is done using a low power ultrasonicator for 15 min. The samples were again cleaned with ethanol in an ultrasonicator for 1 min and placed inside the cold walled aluminum chamber of hot filament chemical vapor deposition system (sp^3 Diamond Technologies Inc., USA). An array of 31 parallel

wires of (0.12 mm) diameter filaments, with 12 mm wire to wire spacing and stand off distance of 18 mm, was placed above the samples. For acquiring NCD coatings a rotary pump was used to continuously pump the hot filament chemical vapor deposition (HFCVD) chamber. During the preparation of NCD samples the methane (90 sccm) diluted in excess of hydrogen (2250 sccm), were quantified at carefully controlled rates. The assembly of gas distribution allowed the control of the gas flow patterns in and around the filament assembly and the sample to ensure uniformness in the coatings. For deposition of NCD coatings, the set chamber pressure during the deposition was 7 Torr, which was maintained accurately by a throttle valve connected to the rotary pump. A two color pyrometer monitored the temperature of tungsten filament. It was found to be 2200 °C. A *k*-type thermocouple was used to measure the temperature of titanium alloy samples. The thermocouple was located beneath the titanium alloy samples. It was found to be 800 °C. The whole growth process was performed for 3 h and the thickness of the film was estimated to be 3 μm.

In a separate experiment, for the purpose of acquiring microcrystalline diamond coatings, the methane (45 sccm), diluted in excess of hydrogen (2250 sccm), were quantified in at carefully controlled rates. The set chamber pressure during the deposition was 36 Torr, which was maintained constant throughout the experiment. The third experiment comprised of the same experimental conditions as that of the first one except that a small content of boron (0.5 %) was added to the samples.

Structural characteristics of these coatings were studied using grazing incidence X-ray diffraction (PANalytical) technique with Cu$K\alpha$ ($\lambda = 0.154$ nm) radiation at 3° grazing angle and confocal Raman microscope (Alpha 300R, WITec) at an excitation wavelength of 448 nm. Surface morphology of these coatings were analyzed using a high resolution scanning electron microscope (HRSEM, Quanta 3D, FEI). Friction characteristics were carried out using a ball-on-disc type linear reciprocating micro-tribometer (CSM Instruments, Switzerland) under dry sliding conditions. Alumina (Al_2O_3) ball of size 6 mm was used as sliding ball, applying at three different normal loads of 1, 5 and 10 N. A sliding speed of 8 cm/s, frequency of 2 Hz and a friction stroke length of 5 mm were used for the overall time period of 20 min. The growth parameters are shown in Table 1.

Table 1. Growth parameters for the deposition of NCD and BDNCD coatings

Coating	Process pressure, Torr	CH_4/H_2, ratio, %	Temperature, °C		Boron concentration, %	Duration, hrs
			filament	substrate		
NCD	12	90/2250, 4	2200	800–850	–	3
MCD	36	45/2250, 2	2200	800–850	–	3
BDNCD	12	90/2250, 4	2200	800–850	0.5	3

RESULTS AND DISCUSSIONS

Characterization of doped diamond films by scanning electron microscopy

The surface roughness and microstructure were examined using a field emission SEM (Quanta 3D, FEI). The NCD coating demonstrates a fairly smooth surface that replicates the texture of the substrate surface. A cauliflower type of morphology is generally shown by the (NCD) of CVD diamond coatings. Figure 1, *a* shows the general surface morphology of the (NCD) of the CVD-diamond

coatings. The MCD coating exhibits clear multi-facet diamond crystals. The MCD coatings have rougher surface because of diamond crystals. MCD coatings exhibit columnar structure of grains and faceted form of the surface morphology. The MCD coatings are shown in Fig 1, *b*. Figure 1, *c* shows the boron-doped NCD coatings which are similar in morphology as undoped NCD coatings.

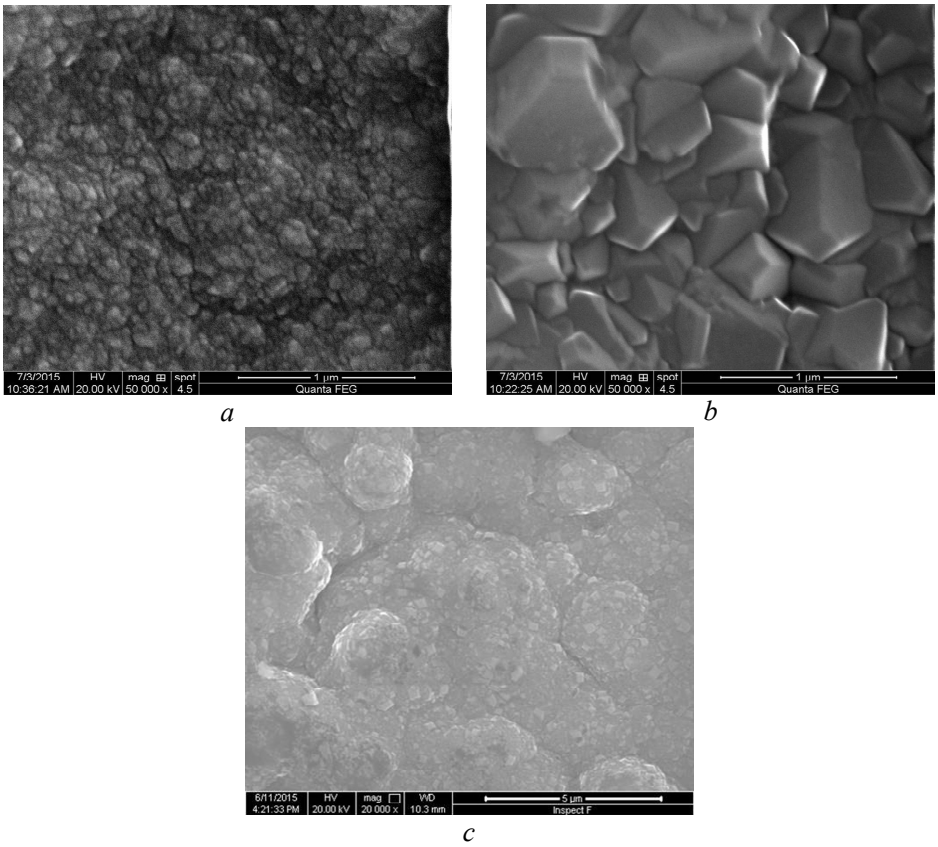

a *b*

c

Fig. 1. Surface morphology of NCD (*a*), MCD (*b*) and boron-doped (*c*) CVD diamond coatings.

XRD analysis

The phase analysis of the deposited films was carried out by X-ray diffraction (X'pert Pro, PANalytical) with Cu*K*α radiation. The XRD patterns of nanocrystalline, microcrystalline and boron-doped nanocrystalline diamond coatings are shown in Figs. 2, *a*, 2, *b*, and 2, *c*, respectively. Sharp and strong peaks of cubic diamond coatings were observed at the (111) crystal and (220) crystal planes at diffraction angles of 44° and 75.5°, respectively, for these coatings, along with the substrate (Ti–6Al–4V) peaks. This confirms the crystallinity of the coatings. Also the variations in these peaks show that its grain size is more than diamond coatings. Since, with the addition of boron content the grain size and lattice parameter of diamond film may be changed.

The average evident sizes of diamond grains along the [111] and [220] directions were obtained by fitting the (111) and (220) diffraction peaks, respectively, and putting on the Scherrer formula [30]:

$$D = \frac{k\lambda}{W_{\text{size}} \cos\theta},$$

where, K is a constant which depends on the specific (hkl) reflection as well as on the grain shape and W_{size} indicates the full width at half maximum (FWHM) because of the influence of size and is given by the following formula:

$$W_{size} = \sqrt{W^2 - W_{IRF}^2} ,$$

W is the FWHM of the calculated diffraction peak and W_{IRF}, the FWHM of the instrumental broadening. In the calculation, K = 1 was assumed. The relative variations of size values are practically significant in this case, and independent calculations were carried out on the (111) and (220) reflections.

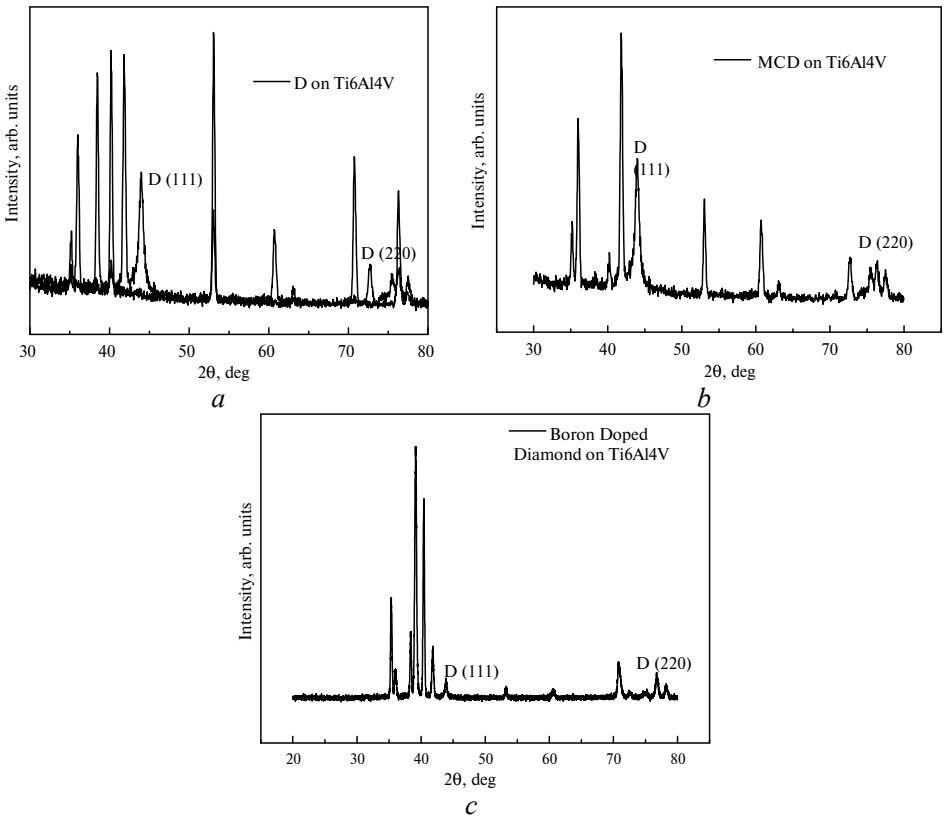

Fig. 2. X-ray diffraction patterns of CVD-diamond coatings: NCD (*a*), MCD (*b*) and boron-doped (*c*) coatings.

Raman spectroscopy and residual stress analysis

Raman spectra of the deposited films were documented using a confocal microscope (Alpha 300, Witec) with an excitation radiation of 448 nm of a Nd:YAG laser activated at less than 20 mW. Raman spectroscopy was used to identify the chemical structure as well as crystalline quality of the diamond coatings. In this respect, stress-free crystalline diamond coating reveals Raman peak at 1332 cm^{-1} corresponding to the first-order phonon mode of T2g symmetry [31]. Raman spectrum of MCD coating confirms the micro-crystallinity. MCD exhibits columnar structure of grains and faceted form of surface morphology. First order Raman peak shift towards higher side centered at 1333 cm^{-1} is indicative of the presence of residual compressive stress in both NCD and MCD coatings. Mainly, this compressive residual stress is due to the difference in thermal expansion coefficients between the substrate and coating [32–35]. Figures 3, *a*, 3, *b* and 3, *c* show the

Raman spectrum of NCD, MCD and boron-doped CVD coatings. Residual stresses can be calculated from $-0.348(\nu_m - \nu_0)$ GPa for fundamental Raman peak at ν_m, where ν_0 =1332 cm^{-1} and ν_m = 1333 cm^{-1}. Thus, both NCD and MCD diamond coating systems contain a compressive stress of –0.348 GPa (the negative sign indicates a compressive stress). In the case of NCD coatings, two other peaks ν_1 and ν_3 are characteristics of in-plane (C–H) and stretching (C–C) vibrational modes, respectively. The existence of these modes was ascribed to the formation of trans-polyacetylene (TPA) chain in the grain boundaries, which is a familiar characteristic of NCD coatings. A cauliflower type of growth is generally seen with the NCD coatings [36–39]. As for boron-doped diamond films, 1332 cm^{-1} peak changes towards an asymmetric Fano effect. The broad bands at around 500 and 1250 cm^{-1} may well be related to the actual boron incorporation in the lattice. Their position accepts with two maxima of the phonon density of states (PDOS) of diamond. The shifts of Raman diamond peak to the higher and lower frequency are corresponded to compressive and tensile stresses in the diamond films, respecttively. Undoped diamond films show compressive stress, whereas tensile in-plane bi-axial stress can be realized in B–doped diamond films. The tensile stress is mostly induced by high defect density in the B–doped diamond films and node-blocked sliding effect at the grain boundary. Residual stresses can be calculated from $-0.348(\nu_m - \nu_0)$ GPa for fundamental Raman peak at ν_m, where ν_0 = 1332 cm^{-1} and ν_m = 1301 cm^{-1}, σ = –0.348(1301 – 1332) GPa. Thus, boron-doped diamond coating system contains a tensile stress of 10.788 GPa, where positive sign indicates tensile stress.

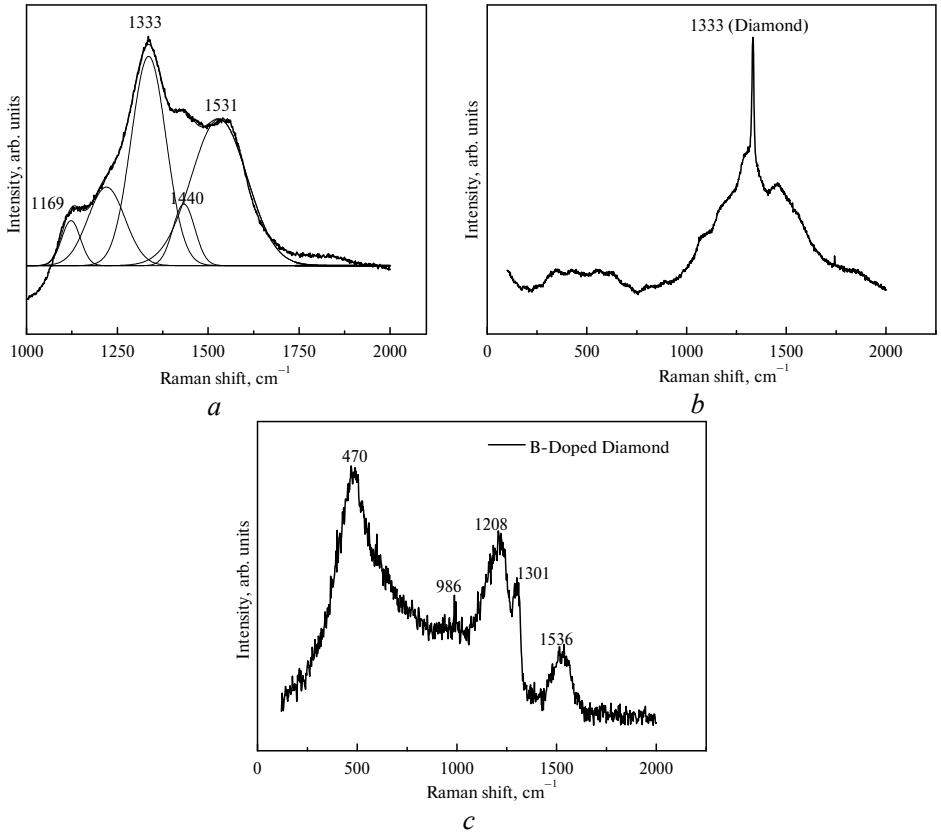

Fig. 3. Raman spectra of CVD-diamond coatings: NCD (*a*), MCD (*b*), boron-doped (*c*) coatings.

Friction characteristics of the NCD, MCD and boron-doped NCD coatings against alumina balls

The friction coefficient curves of NCD, MCD and boron-doped diamond films sliding with Al_2O_3 balls are shown in Figs. 4, 5 and 6, respectively, for a sliding speed of 8 m/s and a load of 1, 5 and 10 N, respectively. Figs. 4, *a*, 5, *a* and 6, *a* show the friction coefficient of NCD, MCD and BDNCD at 1 N, respectively. Figures 4, *b*, 5, *b* and 6, *b* show the friction coefficient of NCD, MCD and BDNCD at 5 N. Figures 4, *c*, 5, *c* and 6, *c* show the friction coefficient of NCD, MCD and BDNCD at 10 N, respectively. Figures 4, *d*, 5, *d* and 6, *d* show the average friction coefficient of NCD, MCD and BDNCD, respectively. Table 2 shows the summary of residual stresses and variation in coefficient of friction. Figure 7 shows the comparison of average coefficient of friction between NCD, MCD and BDNCD coatings. Figure 8, *a*, shows the Raman spectrum of wear track of NCD coatings at 10 N while Figs. 8, *b* and 8, *c* show the Raman spectrum of wear track of MCD and BDNCD CVD diamond coatings at 10 N respectively. Figures 9, *a* and 9, *b* shows the surface morphology of the wear tracks of NCD and MCD coatings at 10 N while Fig. 9, *c* shows the surface morphology of the wear track of boron-doped CVD diamond coatings at 10 N. Figures 10, 11 and 12 show the EDX analysis of NCD, MCD and boron-doped coatings while there compositions are given in Tables 3, 4 and 5 respectively. The loud wavering of the friction coefficient observed at 1N are due to the surface roughness. After a longer test carried out in these conditions, the diamond coating on the disc is found to be intact as shown by

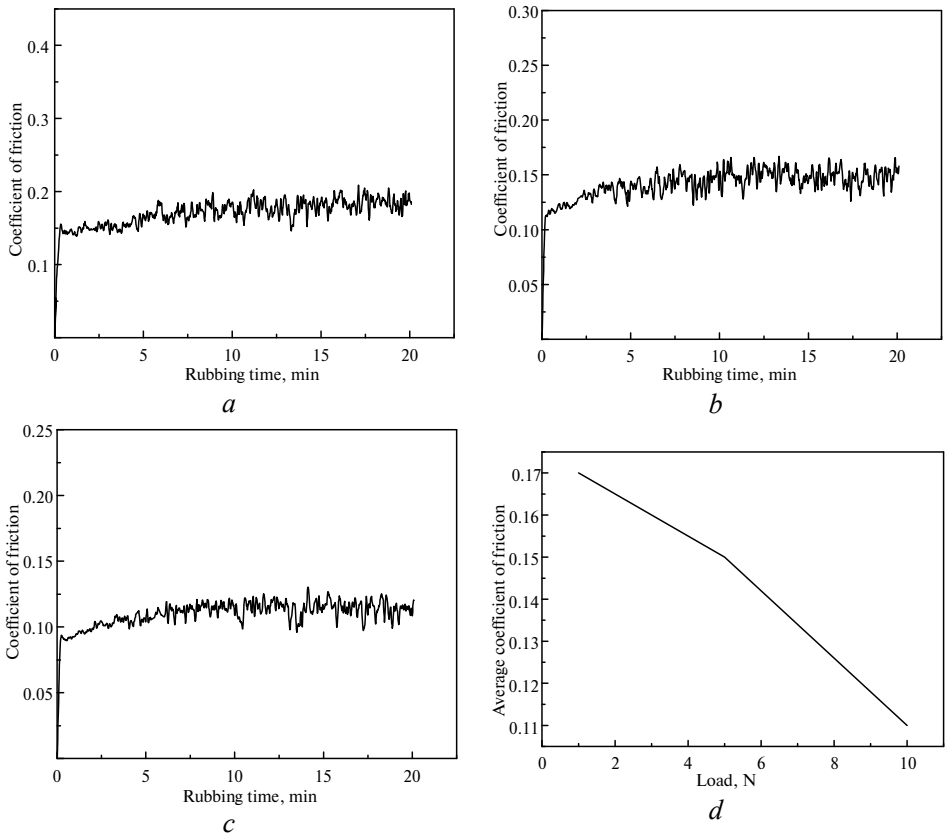

Fig. 4. Tribological characteristics of alumina ball sliding against NCD coating at 1 (*a*), 5 (*b*), 10 (*c*) N and average coefficient of friction (*d*).

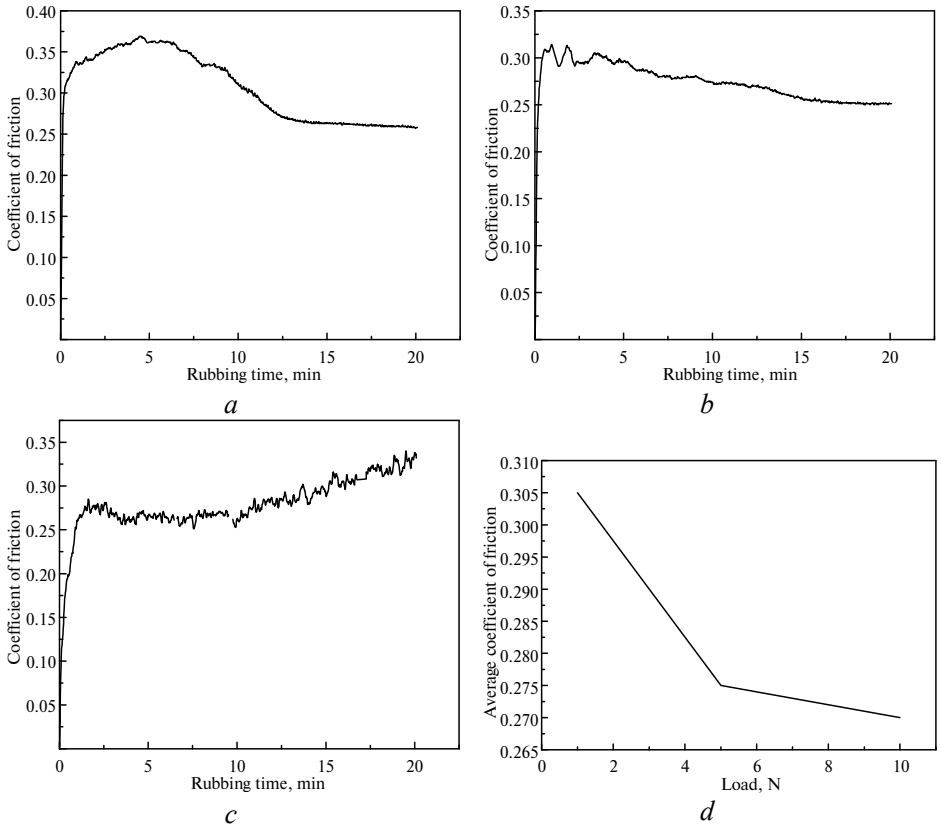

Fig. 5. Tribological characteristics of alumina ball sliding against MCD coating at 1 (*a*), 5 (*b*), 10 (*c*) N and average coefficient of friction (*d*).

the SEM and indicated by the surface roughness values, which remain unchanged. At higher loads, the friction coefficient measured in the same track stabilizes after about 12 min. At the beginning of the applied load we can observe a peak which corresponds to the adaptation of the contact of both counter-faces. At the end of the test carried out at 10 N on the coating a wear track of 230 μm in width was formed on the diamond coated disc. The high magnification image of this area shows that the worn surface is significantly polished. When increasing the time, at a sliding speed of 8 m/s and a load of 10 N, the friction coefficient gradually decreases after a time period of 3 min. After the initial high peak, the curve of boron-doped diamond films first drops to a low value and then increases to some degree before transiting to the steady state. While for undoped diamond films, the coefficient directly transits to the steady state. The boron-doped diamond films demonstrate exceptional tribological property. They show the lowest wear rate of the films and the counterpart ball, followed by undoped diamond films. The adhered transferred materials make the transition regime in the friction coefficient evolution of boron-doped diamond films differ from that of undoped diamond films. Among all the tested diamond films, friction tests suggest that the boron-doped diamond films exhibit the lowest friction coefficient and wear rate, because of its diamond grain refinement effect. A lower friction coefficient is found in boron-doped diamond films than that of undoped ones. No variation of the total volume wear rate as a function of time was evidenced during the test since the vertical movement was negligible, a few micrometers at the end of the test. At this point, the final wear rate of the ball is about

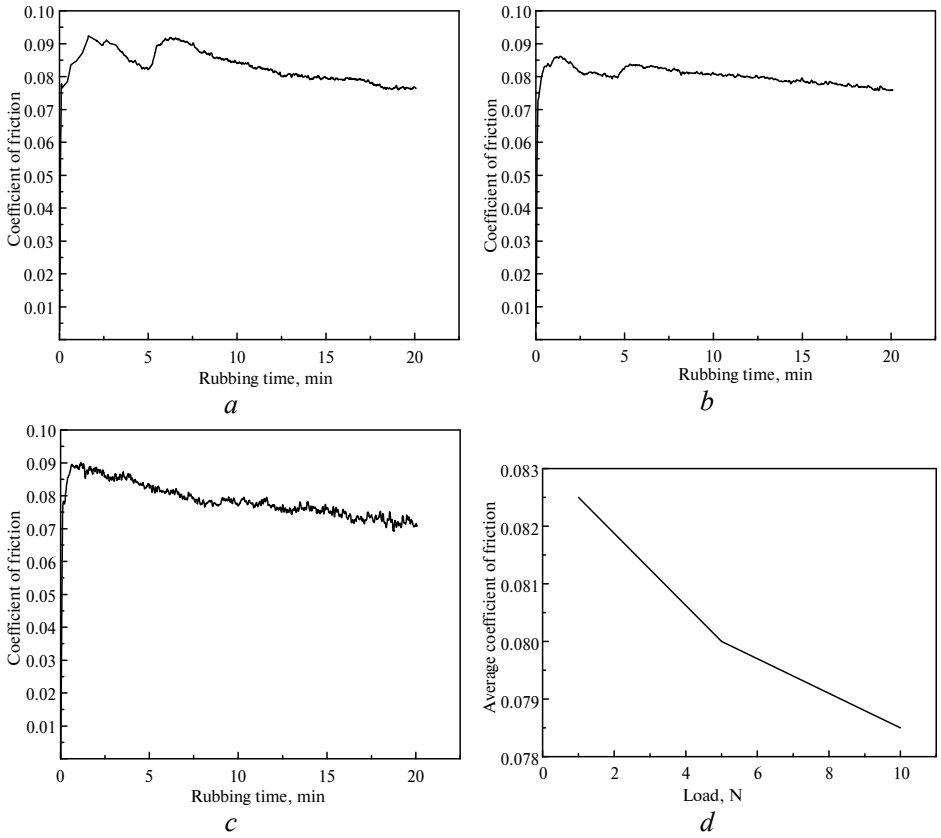

Fig. 6. COF of boron-doped diamond coatings on titanium alloy at 1 (*a)*, 5 (*b*), 10 (*c*) N and average COF (*d*).

5×10^{-17} m^3(N/m). The wear of the diamond coated disc is too low to be measured and the wear track is just polished, as detected by SEM and confirmed by the AFM measurements. This lack of the coating wear of the disc results from the short test duration due to the ball wearing more quickly. Alumina is a chemically inert ceramic compound and sliding interaction of diamond coatings against alumina material is purely mechanical. Low and stable friction coefficient values of around 0.0804 were observed with the boron-doped NCD coating. The stable and low friction coefficient of the boron-doped NCD coating was attributed to the chemical inertness of the mating materials and also due to the continuous availability of the lubricious non-diamond graphitic phases at the grain boundaries of NCD coating. On the other hand, slightly high and unstable friction behavior was observed during the sliding of MCD coating against alumina ball. High run-in friction values of ~ 0.283 (average) were observed with the MCD coatings. The high run-in friction behavior of the MCD coating as compared to the NCD and BDNCD coatings was attributed to its sharp and rough surface asperities. When increasing the time, at a sliding speed of 8 m/s and a load of 10 N, the friction coefficient first increases and then decreases gradually after a time period of 5 min and remains constant after 12 min. The NCD, MCD and doped diamond films undergo similar friction coefficient advancement. Following the initial peak, the coefficient of friction transit to a lower value and at last reaches a steady state. In case of the boron-doped diamond films, the coefficient of friction also starts with a high value but falls to a low value quickly. An increasing regime then can be observed and finally the curve attains a fairly steady state. The averaged friction coefficient is incurred

by undertaking statistics on the data composed after sliding for 20 min. The stable friction coefficient of boron-doped diamond films is lower than that of NCD and MCD diamond films, even though the boron-doped diamond films present larger crystallites and rougher surface. The lower friction coefficient of boron-doped diamond films is due to the interaction mechanism between two contacting surfaces being altered because of a boron incorporation. The boron carbide chemical bonds may exist in the boron-doped diamond films; it would assist in changing the surface frictional energy dissipation and thus change the coefficient of friction [40–43]. The oxide generated by the friction may serve as a solid lubrication, which will help to decrease COF for boron-doped diamond films. The lowest coefficient of friction of 0.0804 is given by boron-doped diamond films. The friction coefficient of B-doped diamond films is lower than that of the undoped diamond films though the B-doped diamond films present bigger crystallites and rougher surface.

Table 2. Tribological results

Coating type	σ (residual stress)	Variation in coefficient of friction
NCD	–0.348 GPa	~ 0.17–0.11
MCD	–0.348 GPa	~ 0.305–0.272
BNCD	10.788 GPa	~ 0.0825–0.0786

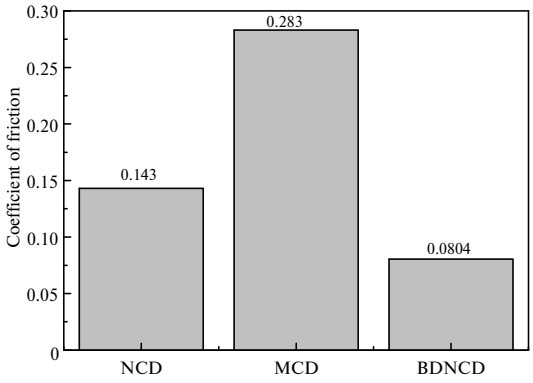

Fig. 7. Comparison of average coefficients of friction of NCD, MCD and boron-doped diamond coatings.

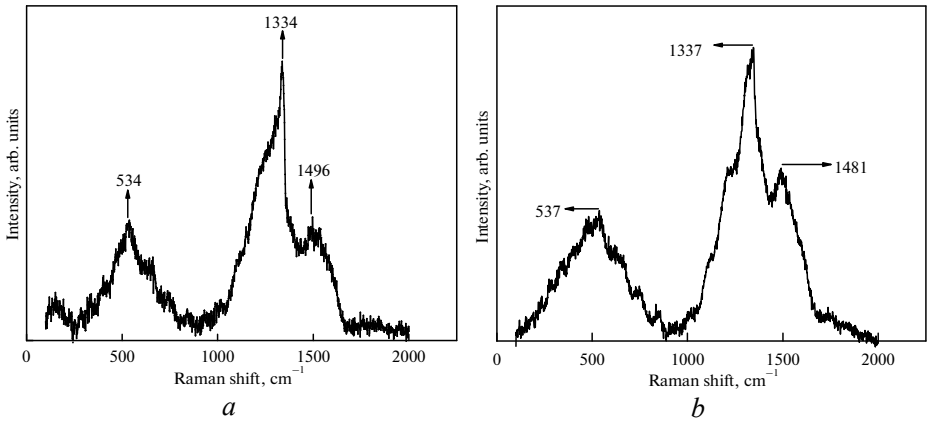

Fig. 8. Raman spectra of wear track of CVD-diamond coatings NCD (*a*), MCD (*b*) and of boron-doped CVD-diamond coatings (*c*).

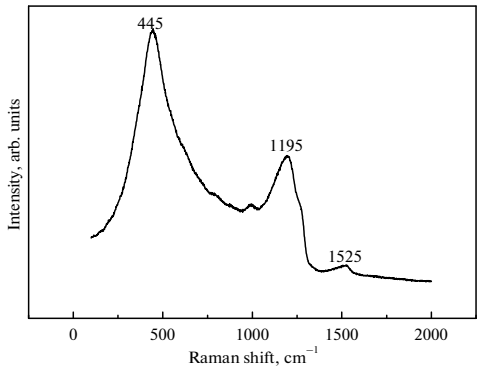

c

Fig. 8. (Contd.)

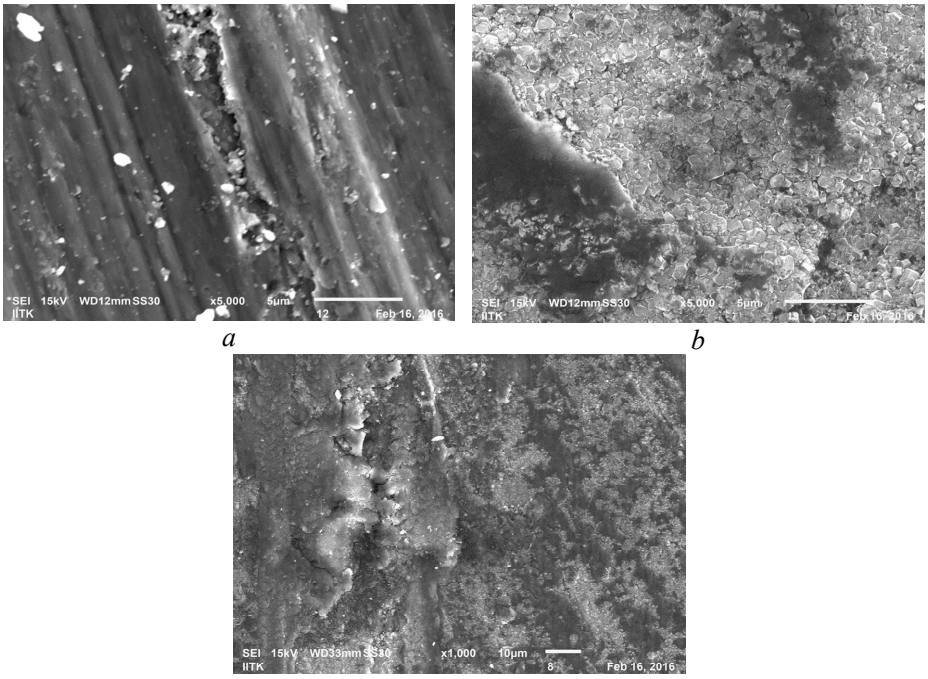

a *b*

c

Fig. 9. SEM images of wear tracks of CVD-diamond coatings: surface morphology of NCD (*a*), MCD (*b*) and boron-doped CVD (*c*) diamond coatings.

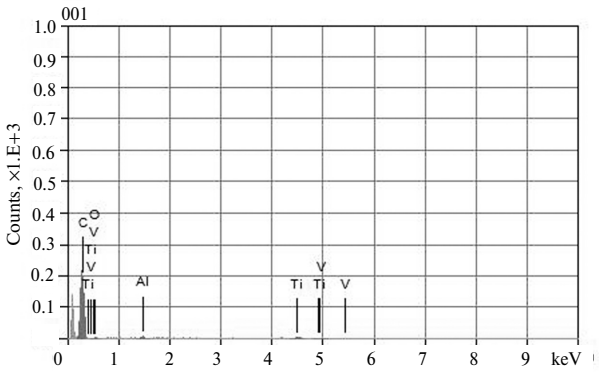

Fig. 10. EDX analysis of wear track of NCD coatings.

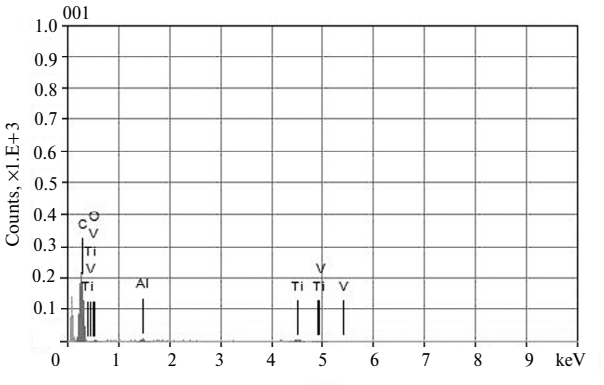

Fig. 11. EDX analysis of wear track of MCD coatings.

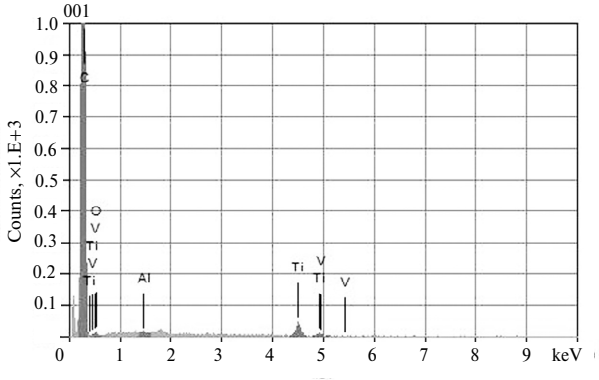

Fig. 12. EDX analysis of wear tracks of boron-doped coatings.

Table 3. Energy dispersive X-ray analysis (EDXA) of NCD coatings

Chemical formula	mass %	at %	Sigma	Net	*K* ratio	Line
C	81.44	88.51	0.08	50488	0.0206980	K
O	11.48	9.37	0.21	2205	0.0030696	K
Al	0.92	0.45	0.04	2880	0.0012868	K
Ti	6.04	1.65	0.08	10117	0.0104212	K
V	0.12	0.03	0.05	177	0.0002055	K
Total	100.00	100.0				

Chemical formula	mass %	mol %	Cation	Sigma	Net	*K* ratio	Line
C	86.63	97.82	0.08	50488	50488	0.0206980	K
Al_2O_3	1.90	0.25	0.08	0.08	2880	0.0012868	K
TiO_2	11.23	1.91	0.15	0.15	10117	0.0104212	K
V_2O_5	0.24	0.02	0.09	0.09	177	0.0002055	K
Total	100.00	100.0					

Table 4. Energy dispersive X-ray analysis (EDXA) of MCD coatings

Chemical formula	wt %	at %	Sigma	Net	*K* ratio	Line
C	92.17	96.13	0.27	5346	0.0019595	K
O	3.12	2.45	0.33	57	0.0000688	K
Al	0.97	0.45	0.13	168	0.0001081	K
Ti	3.72	0.97	0.35	221	0.0004347	K
V	0.02	0.00	0.27	1	0.0000020	K
Total	100.00	100.0				

Chemical formula	wt %	mol %	Cation	Sigma	Net	*K* ratio	Line
C	91.96	98.77	0.00	0.27	5346	0.0019595	K
Al_2O_3	1.83	0.23	4.12	0.24	168	0.0001081	K
TiO_2	6.18	1.00	8.86	0.59	221	0.0004347	K
V_2O_5	0.03	0.00	0.04	0.48	1	0.0000020	K
Total	100.00	100.0					

Table 5. Energy dispersive X-ray analysis (EDXA) of boron-doped coatings

Chemical formula	wt %	at %	Sigma	Net	K ratio	Line
C	94.51	97.86	0.09	52611	0.0192846	K
O	1.33	1.03	0.11	212	0.0002548	K
Al	0.15	0.07	0.03	230	0.0001478	K
Ti	3.79	0.98	0.11	2025	0.0039870	K
V	0.22	0.05	0.08	99	0.0002267	K
Total	100.00	100.0				

Chemical formula	wt %	mol %	Cation	Sigma	Net	K ratio	Line
C	93.18	98.96	0.00	0.09	52611	0.0192846	K
Al_2O_3	0.27	0.03	0.74	0.06	230	0.0001478	K
TiO_2	6.16	0.98	10.71	0.18	2025	0.0039870	K
V_2O_5	0.38	0.03	0.59	0.14	99	0.0002267	K
Total	100.00	100.00	12.04				

CONCLUSIONS

The effect of boron doping on residual stresses and frictional coefficient of CVD diamond coatings has been analyzed. Boron concentration changes the compressive residual stresses to tensile. Further, at a boron content of 0.5 %, there is nearly 43.77 % reduction in friction coefficient. The results of Raman spectra indicate that the boron-doped diamond films present tensile stress while undoped diamond films show compressive stresses. The friction tests reveal that the boron-

doped diamond films presented lower friction coefficient, when sliding with Al_2O_3 ceramic materials, compared to undoped diamond films although boron-doped diamond films have comparatively larger grain size and rougher surface. The average friction coefficient of BDNCD was 0.0804 at different loads when sliding against Al_2O_3 balls, whereas NCD and MCD coatings exhibited a higher value of 0.143 and 0.283, respectively.

ACKNOWLEDGMENT

The authors thank Prof. M. S. Ramachandra Rao, MSRC lab, IIT Madras, for the deposition of coatings and C. Anandan (Surface Engineering Division, NAL, Bangalore, India) for doing tribological tests and Prof. Kamal K. Kar, IIT Kanpur.

Досліджено нанокристалічні, мікрокристалічні і леговані бором нанокристалічні алмазні покриття, нанесені на титановий сплав. Вивчено вплив легування бором на коефіцієнт тертя і залишкові напруги алмазних покриттів. Трибологічні характеристики вищезазначених трьох видів покриттів на підкладках Ti–6Al–4V вивчали з використанням мікротрибометра "куля на диску", товщина покриттів становила 3 мкм. Диски з покриттям Ti–6Al–4V ковзали відносно куль з оксиду алюмінію (Al_2O_3) з нормальним навантаженням від 1 до 10 Н. Легований бором зразок диска з NCD-покриттям мав найнижчий середній коефіцієнт тертя ~ 0,0804, тоді як нелеговані диски з покритями NCD і MCD мали середні коефіцієнти тертя ~ 0,143 і ~ 0,253 відповідно. Дослідження за допомогою рамановскої спектроскопії виявили, що залишкові напруги були за природою такими, що розтягують, тоді як залишкові напруги в нелегованих NCD і MCD виявилися такими, що стискають.

***Ключові слова**: легування бором, CVD алмазні покриття, коефіцієнт тертя.*

Исследованы нанокристаллические, микрокристаллические и легированные бором нанокристаллические алмазные покрытия, нанесенные на титановый сплав. Изучено влияние легирования бором на коэффициент трения и остаточные напряжения алмазных покрытий. Трибологические характеристики вышеупомянутых трех видов покрытий на подложках Ti–6Al–4V изучали с использованием микротрибометра "шар на диске", толщина покрытий составляла 3 мкм. Диски с покрытием Ti–6Al–4V скользили относительно шаров из оксида алюмия (Al_2O_3) с нормальной нагрузкой от 1 до 10 Н. Легированный бором образец диска с NCD-покрытием имел самый низкий средний коэффициент трения ~ 0,0804, тогда как нелегированные диски с покрытиями NCD и MCD имели средние коэффициенты трения ~ 0,143 и ~ 0,253 соответственно. Исследования с помощью рамановской спектроскопии выявили, что остаточные напряжения были по природе растягивающими, тогда как остаточные напряжения в нелегированных NCD и MCD оказались сжимающими.

***Ключевые слова**: легирование бором, CVD алмазные покрытия, коэффициент трения.*

1. *Liu X., Chu P. K., Ding C.* Surface modification of titanium, titanium alloys, and related materials for biomedical applications // Mater. Sci. Eng. R. – 2004. – **47**. – P. 49–121.
2. *Ganapathy P., Manivasagam G., Rajamanickam A., Natarajan A.* Wear studies on plasma-sprayed Al_2O_3 and 8 mole % of Yttrium-stabilized ZrO_2 composite coating on biomedical Ti–6Al–4V alloy for orthopedic joint application // Int. J. Nanomedicine. – 2015. – **10**. – P. 213–222.
3. *Long M., Rack H. J.* Titanium alloys in total joint replacement-materials science perspective // Biomaterials. – 1998. – **19**, N 18. – P. 1621–1639.
4. *Long M., Rack H. J.* Friction and surface behavior of selected titanium alloys during reciprocating-sliding motion // Wear. – 2001. – **249**, N 1–2. – P. 158–168.
5. *Geetha M., Singh A. K., Asokamani R., Gogia A. K.* Ti based biomaterials, the ultimate choice for orthopaedic implants. A review // Prog. Mater. Sci. – 2009. – **54**, N 3. – P. 397–425.
6. *Kobashi K., Nishimura K., Kawate Y., Horiuchi T.* Synthesis of diamonds by use of microwave plasma chemical-vapor deposition: Morphology and growth of diamond films // Phys. Rev. – 1988. – **38**. – P. 4067–4084.

7. *Johnson C. E., Weimer W. A., Cerio F. M.* Efficiency of methane and acetylene in forming diamond by microwave plasma assisted chemical vapor deposition // Mater. Res. – 1992. – **7**. – P. 1427.
8. *Martin L. R., Hill M. W.* A flow-tube study of diamond film growth: methane versus acetylene // Mater. Sci. Lett. – 1990. – **9**. – P. 621.
9. *Ohtake N., Yoshikawa M.* Diamond film preparation by arc discharge plasma jet chemical vapor deposition in the methane atmosphere // Electrochem. Soc. – 1990. – **137**. – P. 717.
10. *Niu C.-M., Tsagaropoulos G., Baglio J., Dwilight K., Wold A.* Nucleation and growth of diamond on Si, Cu, and Au substrates // Solid State Chem. – 1991. – **91**. – P. 47.
11. *Jansen F., Machonkin M., Kuhman D.* The deposition of diamond films by filament techniques // Vacuum J. Sci. Technol. A. – 1990. – **8**. – P. 3785.
12. *Fayeulle S., Blanchard P., Vincent L.* Fretting behavior of titanium alloys // Tribol. Transact. – 1993. – **36**. – P. 267.
13. *Budinski K. G.* Wear of Materials // ASME, Conf. Proc. – Orlando, Florida, 1991. – 289 p.
14. *Lutynski C., Simansky G., MvEvily A. J.* Materials Evaluation under Fretting Conditions. – ASTM, Philadelphia, 1982. – 150 p.
15. *Grogler T., Franz A., Klaffke D., Rosiwal S. M., Singer R. F.* Tribological optimization of CVD diamond coated Ti–6Al–4V // Diamond Relat. Mater. – 1998. – **7**. – P. 1342–1347.
16. *Grogler T., Plewa O., Rosiwal S. M., Singer R. F.* Microwave-plasma-CVD of diamond coatings onto titanium and titanium alloys // Surf. Coat. Technol. – 1998. – **98**. – P. 1079–1091.
17. *Haubner R., Bohr S., Lux B.* Comparison of P, N, and B additions during CVD diamond deposition // Diamond Relat. Mater. – 1999. – **8**. – P. 171–178.
18. *Werner M., Lochar R.* Growth and application of undoped and doped diamond films // Reports on Progress in Physics. – 1998. – **61**. – P. 1665–1710.
19. *Kalss W., Bohr S., Haubner R., Lux B., Griesser M., Spicka H., Grasserbauer M., Wurzinger P.* Influence of boron on diamond growth on WC–Co hard-metals // Int. J. Refract. Mater. – 1996. – **14**. – P. 137–144.
20. *Haubner R.* Comparison of sulfur, boron, nitrogen, and phosphorus additions during low-pressure diamond deposition // Diamond Relat. Mater. – 2005. – **14**. – P. 355–363.
21. *Zhang R. J., Lee S.T., Lam Y. W.* Characterization of heavily boron-doped diamond films // Ibid. – 1996. – **5**. – P. 1288–1294.
22. *Wang Z. L., Lu C., Li J. J., Gu C. Z.* Influence of growth pressure on the electrical properties of boron-doped polycrystalline diamond films // Appl. Surf. Sci. – 2009. – **255**. – P. 9522–9525.
23. *Wang L., Lei X., Shen B., Sun F., Zhang Zh.* Tribological properties and cutting performance of boron- and silicon-doped diamond films on Co-cemented tungsten carbide inserts // Diamond Relat. Mater. – 2013. – **33**. – P. 54–62.
24. *Colley L., Williams C. G., Johansson U. D., Newton M. E., Unwin P. R. Wilson N. R., Macpherson J. V.* Examination of the spatially heterogeneous electroactivity of boron-doped diamond microarray electrodes // Anal. Chem. – 2006. – **78**. – P. 2539.
25. *Pleskov Y. V.* New corrosion-resistant electrodes: Synthetic diamond and diamond-based materials. The semiconductor and structure aspects // A review, Prot. Met. – 2006. – **42**. – P. 103.
26. *Suffredini H. B., Salazar-Banda G. R., Tanimoto S. T., Calegaro M. L., Machado S. A. S., Avaca L. A.* AFM studies and electrochemical characterization of boron-doped diamond surfaces modified with metal oxides by the Sol-Gel method // J. Brazilian Chem. Soc. – 2006. – **17**. – P. 257–264.
27. *Xie S. T., Shafer G., Wilson C. G., Martin H. B.* In vitro adenosine detection with a diamond-based sensor // Diamond Relat. Mater. – 2006. – **15**. – P. 225.
28. *Balducci A., D'amico A., Di Natale C., Marinelli M., Milani E., Morgada M. E., Pucella,G., Rodriguez G., Tucciarone A., Verona-Rinati G.* High performance CVD-diamond-based thermocouple for gas sensing // Sensors Actuat. B: Chem. – 2005. – **111–112**. – P. 102.
29. *Ferreira N. G., Silva L. L. G., Corat E. J., Trava-Airold V. J.* Kinetics study of diamond electrodes at different levels of boron doping as quasi-reversible systems // Diamond Relat. Mater. – 2002. – **11**. – P. 1523.
30. *Langford J. I., Wilson A. J. C.* Scherrer after sixty years: a survey and some new results in the determination of crystallite size // J. Appl. Crystallogr. – 1978. – **11**. – P. 102.
31. *Hou Y. Q., Zhuang D. M., Zhang G., Wu M. S., Liu J. J.* Tribological performances of diamond film and graphite/diamond composite film // Wear. – 2002. – **253**. – P. 711.

32. *Sarangi S. K., Chattopadhyay A., Chattopadhyay A. K.* Effect of pretreatment methods and chamber pressure on morphology, quality, and adhesion of HFCVD diamond coating on cemented carbide inserts // Appl. Surf. Sci. – 2008. – **254**. – P. 3721.
33. *Silva F. J. G., Fernandes A. J. S., Costa F. M., Baptista A. P. M., Pereira E.* A new interlayer approach for CVD diamond coating of steel substrates // Diamond Relat. Mater. – 2004. – **13**. – P. 828.
34. *Seo S. H., Lee T. H., Park J. S.* Roughness control of polycrystalline diamond films grown by bias-enhanced microwave plasma-assisted CVD // Ibid. – 2003. – **12**. – P. 1670.
35. *May P. W., Ludlow W. J., Hannaway M., Heard P. J., Smith J. A., Rosser K. N.* Raman and conductivity studies of boron-doped microcrystalline diamond, facetted nanocrystalline diamond, and cauliflower diamond films // Chem. Phys. Lett. – 2007. – 446. – P. 103–108.
36. *Sun F., Ma Yu., Shen B., Zhang Zh., Chen M.* Fabrication and application of nano.microcrystalline composite diamond films on the interior hole surfaces of Co cemented tungsten carbide substrates // Diamond Relat. Mater. – 2009. – **18**. – P. 276–282.
37. *Polini R., Traversa E., Marucci A., Mattei G., Marcheselli G.* A Raman study of diamond film growth on Co-cemented tungsten carbide // Electrochem. Soc. – 1997. – **144**. – P. 1371–1375.
38. *Kulisch W., Popov C.* On the growth mechanisms of nanocrystalline diamond films // Phys. Status Solidi A. – 2006. – **203**. – P. 203–219.
39. *Wang W. L., Polo M. C., Sanchez G., Cifre J., Esteve M.* Internal stress and strain in heavily boron-doped diamond films grown by microwave plasma and hot filament chemical vapor deposition // J. Appl. Phys. – 1996. – **80**. – P. 1846–1850.
40. *Liang Q., Stanishevsky A., Vohra Y. K.* Tribological properties of undoped and boron-doped nanocrystalline diamond films // Thin Solid Films. – 2008. – **517**. – P. 800–804.
41. *Archard J. F.* Single contacts and multiple encounters // J. Appl. Phys. – 1961. – **32**. – P. 1420–1425.
42. *Yan Ch.-Sh., Mao H.-Kw., Li W., Qian J., Zhao Yu., Hemley R. J.* Ultrahard diamond single crystals from chemical vapor deposition // Phys. Stat. Sol. – 2004. – **201**, P. R25–R27.
43. *Li X. M, Wang J. D, Chen D. R, Liu B, Liu F. B*. Mechanical properties of diamond thin films characterised by nano-indentation method // J. Chinese Ceram. Soc. – 2005. – **33**. – P. 1539–1543.

Received 14.06.16